Geobiology (2013), **11**, 593–601 DOI: 10.1111/gbi.12061

Iron reduction and mineralization of deep-sea iron reducing bacterium *Shewanella piezotolerans* WP3 at elevated hydrostatic pressures

W. F. WU,[1,2] F. P. WANG,[3] J. H. LI,[1,2] X. W. YANG,[3] X. XIAO[3] AND Y. X. PAN[1,2]

[1]*Biogeomagnetism Group, Paleomagnetism and Geochronology Lab, Key Laboratory of the Earth's Deep Interior, Institute of Geology and Geophysics, Chinese Academy of Sciences, Beijing, China*
[2]*France-China Bio-Mineralization and Nano-Structures Laboratory, Chinese Academy of Sciences, Beijing, China*
[3]*State Key Laboratory of Ocean Engineering, State Key Laboratory of Microbial Metabolism, Shanghai Jiao Tong University, Shanghai, China*

ABSTRACT

In this study, iron reduction and concomitant biomineralization of a deep-sea iron reducing bacterium (IRB), *Shewanella piezotolerans* WP3, were systematically examined at different hydrostatic pressures (0.1, 5, 20, and 50 MPa). Our results indicate that bacterial iron reduction and induced biomineralization are influenced by hydrostatic pressure. Specifically, the iron reduction rate and extent consistently decreases with the increase in hydrostatic pressure. By extrapolation, the iron reduction rate should drop to zero by ~68 MPa, which suggests a possible shut-off of enzymatic iron reduction of WP3 at this pressure. Nano-sized superparamagnetic magnetite minerals are formed under all the experimental pressures; nevertheless, even as magnetite production decreases, the crystallinity and grain size of magnetite minerals increase at higher pressure. These results imply that IRB may play an important role in iron reduction, biomineralization, and biogeochemical cycling in deep-sea environments.

Received 29 January 2013; accepted 20 August 2013

Corresponding author: Y. X. Pan. Tel.: +86 10 8299 8406; fax: +86 10 6201 0846; e-mail: yxpan@mail.iggcas.ac.cn

INTRODUCTION

Iron reducing bacteria (IRB) are capable of coupling Fe (III) reduction to organic carbon oxidation as an energy yielding process that induces the precipitation of iron minerals (Lovley *et al.*, 2004). Through this process, IRB exert a significant control on iron migration and precipitation pathways and may have extensively participated in the Precambrian biogeochemical cycle of iron (e.g., Konhauser *et al.*, 2005; Johnson *et al.*, 2008; Heimann *et al.*, 2010; Li *et al.*, 2011). IRB broadly inhabit the Earth's terrestrial subsurface and deep-sea environments. Picard *et al.* (2012) studied the effects of pressure on iron reduction by *Shewanella oneidensis* MR-1 isolated from lake sediments. They found that the initial rate of iron reduction increased with pressure up to 40 MPa, while the initial Fe(III) provided (5 mM) was reduced at pressures up to 70 MPa, suggesting that IRB might contribute to iron cycling in deep-sea environments. Furthermore, several piezotolerant IRB have been isolated in the deep-sea sediments at water depths ranging from 1000 to 5000 m (Xu *et al.*, 2003; Toffin *et al.*, 2004; Stapleton *et al.*, 2005), equivalent to hydrostatic pressures (HP) of 10–50 MPa.

Dissimilatory iron reduction by IRB in deep sea serves as important processes of transforming iron and precipitating nano-sized iron minerals (Lovley, 1997; Slobodkin *et al.*, 2001; Roh *et al.*, 2006). In deep-sea environment, the metabolic behavior of IRB can be strongly affected by HP conditions, as discussed above. However, the concomitant biologically induced mineralization processes under high pressure have not yet been systematically examined. Experimental investigations of iron reduction and mineralization of marine IRB under various pressures will allow us to better understand the extent of IRB contribution to iron cycling in deep-sea settings.

Recently, we found that deep-sea IRB *Shewanella piezotolerans* WP3 (hereafter WP3) could effectively reduce ferrihydrite and induce the mineralization of superparamagnetic magnetite particles at 0.1 MPa and 20 °C (Wu *et al.*, 2011). Under these experimental conditions, the metabolic activity of WP3 quickly altered the initial near neutral culturing medium to an alkaline and reduced environment, which favors the precipitation of magnetite (Wu *et al.*, 2011). In the present study, a combination of X-ray diffraction (XRD), transmission electron microscopy (TEM), and rock magnetism was used to examine the iron reduction rates and total extent reduction by WP3, and the concomitant biomineralization products under different HP conditions (0.1, 5, 20 and 50 MPa), and possible mechanisms for the HP effects are discussed.

MATERIALS AND METHODS

Bacterial strain and culture medium

Shewanella piezotolerans WP3 was isolated from West Pacific sediments at a water depth of ~1914 m (Xiao *et al.*, 2007; Wang *et al.*, 2009). In this study, cells were grown in 2216 Marine Medium (5 g peptone, 1 g yeast extract, 0.01 g $FePO_4$, 34 g NaCl in 1-L water) in a shaker at a rotation speed of 250 rpm at 20 °C and 0.1 MPa. Cells were harvested in exponential phase, washed, resuspended in anoxic sterile 3.4% NaCl solution, and then a 2% inoculum was transferred to anoxic medium (Wu *et al.*, 2011). Sodium lactate was used as electron donor and carbon source. The medium was buffered with 20 mM HEPES, and the pH was adjusted to 7.50. Ferrihydrite was synthesized (Wu *et al.*, 2011) and added to the medium at a final Fe(III) concentration of 15 mM. Initial cell numbers were 2.3×10^7 cells mL^{-1} as determined by colony-forming units (CFUs) counted on agar plates (1.5% agar) of 2216 Marine Medium. Upon initial inoculation, the medium was immediately dispensed into several 2-mL sterile syringes and placed into the high-pressure vessels and pressurized. The headspace gas (N_2) in the syringe and needle was removed by fully filling with culturing medium, and the needle end of the syringe was sealed with sterile rubber stopper. Cells were grown at 20 °C under pressures of 5, 20, and 50 MPa, which correspond to water depths of approximately 500, 2000, and 5000 m, respectively. Comparative experiments at atmospheric pressure (~0.1 MPa) were also conducted. Abiotic controls without inoculum were also performed at the four experimental pressures (0.1, 5, 20, and 50 MPa).

Hydrostatic pressure system

A sketch of the high HP system used in experiments is shown in Fig. 1. It is composed of a hand-operated pump,

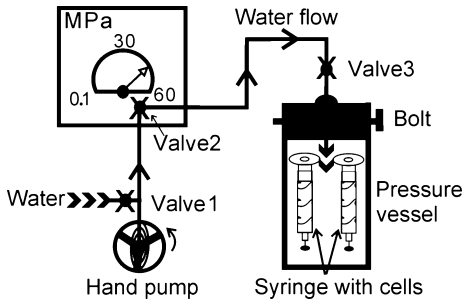

Fig. 1 A sketch of the high hydrostatic pressure system used in this study.

a quick-fit connector, and high HP vessels, which can reach a maximum pressure of 60 MPa. Each pressure vessel holds three parallel experimental syringes and one abiotic control. Before pressurizing, the tube between Valve 1 and Valve 2 was filled with water. The HP vessel is pressurized by injecting water through the quick-fit water pipe. Once at the required pressure, Valve 3 is closed and the water pipe disconnected. The pressurized vessels are then placed into the 20 °C incubators. The pressure vessel can be completely pressurized in less than 90 s with a pressurization rate of ~1 MPa s^{-1} below 30 MPa, and ~0.5 MPa s^{-1} above 30 MPa. This procedure effectively prevents significant biological iron reduction prior to the first measurement. To evaluate possible effects of depressurization on subsequent iron reduction and mineralization, one independent pressure vessel was depressurized (<5 s) and sacrificed for solution chemistry determination and mineral examination at each sampling step.

Fe(II) concentration and cell number determination

The extent and rate of Fe(III) reduction and cell growth rates were monitored for up to 72 h during incubation. The concentration of 0.5 M HCl-extractable Fe(II) was measured by ferrozine assay according to Stookey (1970) on an UV-VIS spectrophotometer (UV-2550; SHIMADZU Corp., Kyoto, Japan). The initial Fe(II) concentration determined by ferrozine assay was 28.5 ± 1.9 μM. Live cell numbers were obtained by counting the CFUs after serial dilutions were spread on agar plates of 2216 Marine Medium.

Magnetic properties measurements

Rock magnetism is a fast, sensitive, non-destructive, and quantitative approach for monitoring IRB mineralization of magnetic minerals. Room- (~20 °C) and low-temperature magnetic measurements were conducted on products formed after 72 h of pressure incubation to examine effects of HP on WP3 biomineralization. Cultures were first centrifuged, and then the pellets were vacuum freeze-dried using a Christ Freeze Dryer ALPHA 1-2 LDplus (Osterode am Harz,

Germany). Room-temperature hysteresis loops were measured by applying a maximum Þeld of ±1.5 T on a Model 3900 vibrating sample magnetometer (VSM) (Princeton Measurements Corp., Westerville, OH, USA), which has a sensitivity of 5×10^{-10} Am^2. Low-temperature hysteresis loops (±3 T) were conducted at 5 K on a Quantum Design Magnetic Property Measurement System (MPMS XL-5), which has a sensitivity of 5×10^{-11} Am^2. Low-temperature magnetization curves were measured from 5 to 300 K in a magnetic Þeld of 40 mT after the samples were cooled down from 300 to 5 K in the absence of a magnetic Þeld [zero-Þeld cooling (ZFC)] and in the presence of a 40 mT Þeld [Þeld cooling (FC)], respectively.

XRD and TEM analyses

The biominerals formed after 120 h of pressurized incubation were analyzed using XRD and TEM techniques to examine HP effects on the mineral assemblages after long-time incubation. Samples were washed with anoxic water to remove residual salts and dried in an anaerobic chamber. XRD was conducted with an XÕPert PRO X-ray Diffractometer at a scan speed of $0.1°s^{-1}$ with a current of 40 mA and a voltage of 40 kV using monochromatic Cu Kα radiation. To investigate the effects of pressure on the lattice chemistry of the biomineralization products, the lattice constants of products were estimated by extrapolating the apparent cell-unit dimension ($d = \lambda \times (h^2+k^2+l^2)^{1/2} / (2 \times \sin\theta)$) along the Nelson–Riley function ($0.5 \times \cos^2\theta/\sin\theta + \cos^2\theta/\theta$) to a 90° Bragg angle (Nelson & Riley, 1945). High-resolution (HR) TEM observation and selected area electron diffraction (SAED) pattern were conducted on a JEM-2100 (JEOL, Tokyo, Japan) microscope at an accelerating voltage of 200 kV.

RESULTS

Bacterial iron reduction and cell growth

At the four experimental pressures (0.1, 5, 20, or 50 MPa), bacterial iron reduction proceeded continuously, while the Fe(II) concentration in abiotic controls remained nearly undetectable during the 72-h incubation (Fig. 2A). However, the extent of Fe(III) reduction at 72 h consistently decreased with the increase in pressure. For example, after 72-h incubation approximately 5.5, 4.8, 4.1, and 1.6 mM Fe(II) were produced at 0.1, 5, 20, and 50 MPa, respectively. Averaged Fe(III) reduction rates at the four pressure conditions, which were calculated by linear regression of the Fe(II) versus time curve, were 79.4, 76.5, 59.0, and 21.1 $\mu M\ h^{-1}$, respectively. By extrapolation, the iron reduction rate dropped to zero by ~68 MPa (Fig. 2B), which is equivalent to a water depth of ~6800 m. This suggests a possible shut-off of enzymatic iron reduction of WP3 under this pressure.

Figure 3 shows the change of CFUs as a function of time. Patterns of cell growth with time at different pressures are similar. Under the four pressure conditions CFUs Þrst

A B

Fig. 2 Time and pressure dependences of iron reduction (Fe(II) concentration) by WP3 under hydrostatic pressures of 0.1 MPa (circles), 5 MPa (triangles), 20 MPa (squares), and 50 MPa (diamonds) (A), and the correlation between the Fe(III) reduction rate and the hydrostatic pressure (B). Experiments were conducted at 20 °C. Fe(II) represents the 0.5 M HCl-extractable Fe(II) concentration. Abiotic control (without inoculation) at 50 MPa were shown in open diamonds in (A).

increased up to 12–18 h, and then decreased until 72 h, which indicates that strain WP3 is viable at pressures up to 50 MPa, although pressure exerts a clear negative influence on cell growth rates. At 50 MPa, CFU number doubled in 12-h incubations and then declined, while at 0.1 MPa, CFU number increased by two orders of magnitude before declining at 18 h. Specific cell growth rates at 0.1, 5, 20, and 50 MPa were ~0.36, 0.32, 0.29, and 0.06 h^{-1}, respectively.

Rock magnetic properties

Room- and low-temperature hysteresis loops

Room-temperature hysteresis loops (Fig. 4) showed typical behaviors of superparamagnetic (SP) particles (Moskowitz *et al.*, 1993), which suggests that the magnetic biomineral products at the four pressures are nano-sized ferrimagnetic minerals, likely magnetite with grain size <20–30 nm (Muxworthy & Williams, 2008). The saturation magnetization (M_s) value, an indicator of the amount of magnetic mineral (Dearing *et al.*, 1997), decreased with increasing pressure. For example, the M_s for the products of 0.1, 5, 20, and 50 MPa after 72-h HP incubation were 32.5, 18.0, 11.4, and 0.06 $Am^2\ kg^{-1}$, corresponding to magnetite concentrations of approximately 35.3%, 19.6%, 12.4%, and 0.07%, respectively. The 'noised' loop for the 50 MPa sample (Fig. 4B) implies the dominance of ferrihydrite in the sample.

Low-temperature hysteresis loops measured at 5 K of samples are shown in Fig. 5. All samples showed pot-bellied loops as the magnetic spin was effectively blocked at low temperature. The M_s for the 0.1 MPa products was 62.7 $Am^2\ kg^{-1}$. It dropped down to 25.6, 18.2, and 10.1 $Am^2\ kg^{-1}$ for 5, 20, and 50 MPa products, respectively. The saturation remanence (M_{rs}) also showed a similar decreasing trend, indicating decrease in magnetite content. The coercive force (B_c) and coercivity of remanence (B_{cr}), dependent on the magnetic domain state, magnetic interaction, and mineralogy, varied systematically. For example, B_c increased from 40.6 mT at 0.1 MPa to 158 mT at 50 MPa, while B_{cr} increased from 58.6 mT at 0.1 MPa to 545 mT at 50 MPa. The biomineral products formed at 50 MPa after 72 h HP incubation had the lowest M_s and M_{rs}, and the highest B_c and B_{cr} values, indicating low magnetite concentration, the mineralogy rather dominated by ferrihydrite.

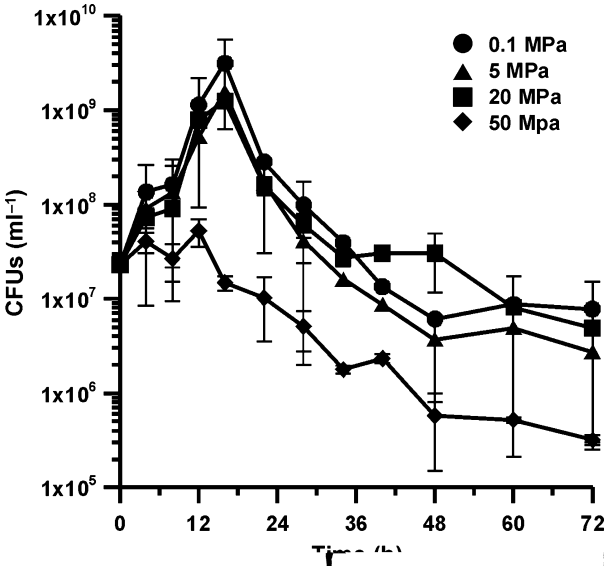

Fig. 3 Time and pressure dependences of WP3 cell growth on ferrihydrite under hydrostatic pressures of 0.1, 5, 20 and 50 MPa. The live cell number is determined by agar plate colony-forming units (CFUs) counting.

Low-temperature magnetization curves

Figure 6 shows the low-temperature (5–300 K) magnetization curves of the four HP samples. On FC curves, the magnetization decreased monotonically with temperature for the 0.1 and 5 MPa samples (Fig. 6A,B) while for the 20 MPa products, it decreased slowly up to 50 K and then dropped rapidly (Fig. 6C). The 50 MPa sample showed a clear concave shape around 30 K (Fig. 6D). On ZFC curves, magnetization first increased before decreasing. The peak temperature (T_p) of the ZFC curves can be used to estimate the average grain size of magnetite (Madsen *et al.*, 2008). The T_p values for 0.1, 5, 20, and 50 MPa products were 78.7, 73.5, 47.7, and 31.2 K, respectively. Nevertheless, the samples consisted of a mixture of magnetite and ferrihydrites, which complicated the interpretation of T_p values in terms of grain sizes.

XRD and TEM results

X-ray diffraction patterns showed that magnetite crystals were formed by 120-h incubation at the four pressures (Fig. 7 and Table 1). The peak intensity, width and position in the XRD pattern changed consistently with pressure. For example, as the pressure increased from 0.1 to 50 MPa, the intensity (units in relative counts) for the (311) peak increased from 48.8 to 112.3, while the full width at half maximum height (FWHM) of the peak decreased from 1.0370° to 0.9193°, and the magnetite lattice constants calculated by Nelson–Riley extrapolation (Nelson & Riley, 1945) decreased from 8.4059 to 8.3876 Å. Taken together with rock magnetic analysis, these likely suggest an increase in crystallinity for the magnetite products with pressure.

HR-TEM observation clearly showed nano-sized (~4–8 nm in diameter) magnetite crystals in samples. Crystal lattices of magnetite were discerned in the HR-TEM images (Fig. 8). We also noted that magnetite formed at high pressures has a larger grain size and a better defined crystal lattice (Fig. 8). No siderite was detected by TEM or XRD analyses.

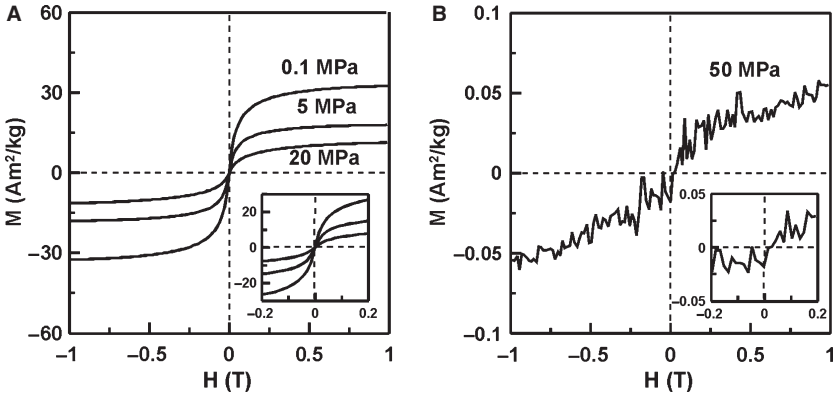

Fig. 4 Hysteresis loops (after paramagnetic correction) of biominerals (72 h products) measured at room temperature. Biominerals were precipitated by WP3 under hydrostatic pressures of 0.1, 5, 20 MPa (A), and 50 MPa (B). *M*, magnetization (Unit: Am^2kg^{-1}); *H*, applied magnetic field (Unit: Tesla).

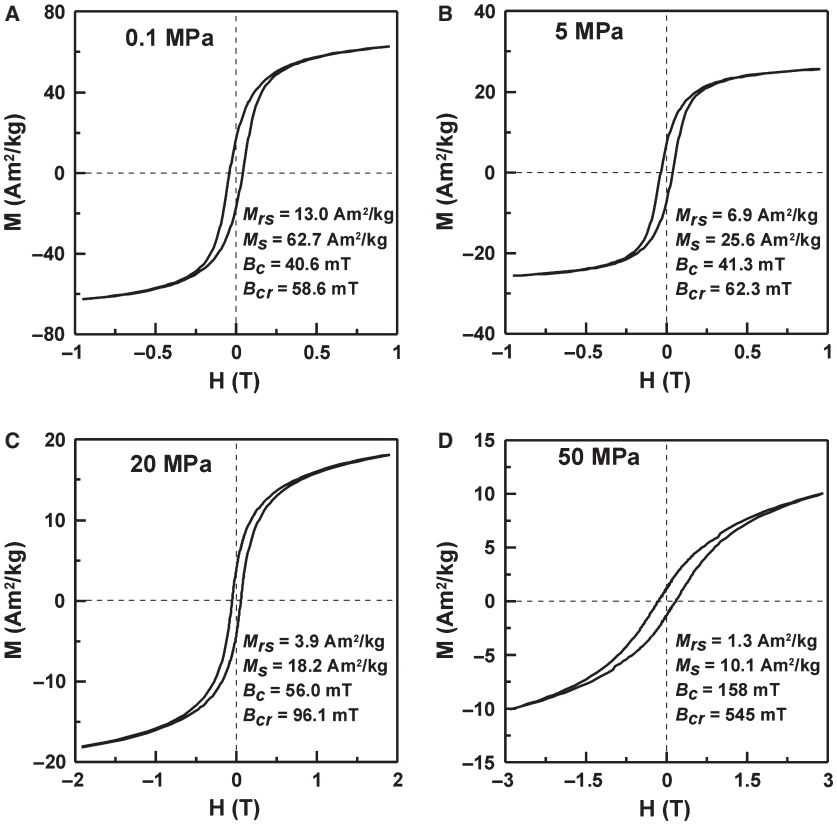

Fig. 5 Hysteresis loops of biominerals (72 h products) measured at 5 K. Biominerals were precipitated by WP3 under hydrostatic pressures of 0.1, 5, 20, and 50 MPa. M_{rs}, saturation remanence; M_s, saturation magnetization; B_c, coercive force; B_{cr}, remanence coercivity.

DISCUSSION AND CONCLUSIONS

Effects of hydrostatic pressures on iron reduction of WP3

Results show that ferrihydrite is biologically reduced by WP3 at the four experimental pressures (Fig. 2), indicating a strong adaptability of WP3 to high-pressure stimuli and the ability of this strain to reduce iron at high pressures.

For a chemical reaction, effects of pressure can be expressed by the principle of Le Chatelier, that is, elevated pressure favors a chemical reaction that produces a volume decrease. Ferrihydrite reduction by WP3 with sodium lactate as electron donor is accompanied with a volume increase by the production of CO_2 as expressed by equation below:

$$12\mathrm{Fe(III)(ferrihydrite)} + \mathrm{C_3H_5O_3^-(lactate)} + 11\mathrm{OH^-} \rightarrow 3\mathrm{CO_2} + 12\mathrm{Fe(II)} + 8\mathrm{H_2O} \quad (1)$$

The decrease in the rate and extent of Fe(III) reduction with pressure may be partially due to this volume increase. As shown in Fig. 3, cell growth rate decreased with pressure, which consequently influences bacterial iron reduction and concomitant iron mineral precipitation (Figs 2, 4

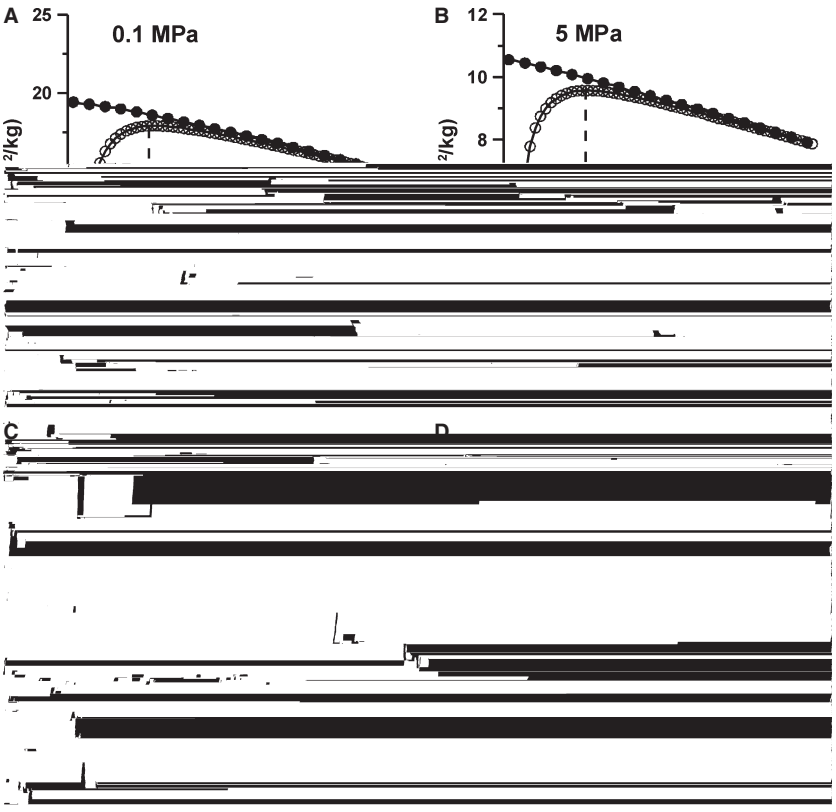

Fig. 6 Low-temperature magnetization curves of biominerals (72 h products) produced by WP3 under hydrostatic pressures of 0.1, 5, 20, and 50 MPa. The magnetization was measured in a magnetic field of 40 mT after the samples were cooled down from 300 to 5 K in the presence field cooling (FC) of a magnetic field (40 mT) and absence of magnetic field (ZFC).

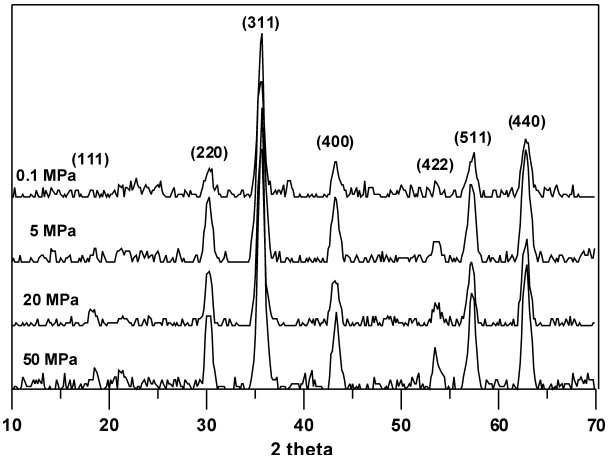

Fig. 7 X-ray diffraction spectra for the biomineralization products of WP3 at 0.1, 5, 20, and 50 MPa after 120-h incubation.

and 5). To further assess the HP effects on bacterial iron reduction, CFU-normalized iron reduction capability at the four pressure conditions was calculated by dividing the total Fe(II) concentration by the corresponding total live cell number, with the assumption that each cell behaved independently during bacterial iron reduction. This yielded CFU-normalized iron reduction rate increase from 3.58×10^{-15} mM CFU^{-1} h^{-1} to 3.11×10^{-14} mM CFU^{-1} h^{-1} as HP increased from 0.1 MPa to 50 MPa (Table 2), indicating that iron reduction by individual cells is still significant at high pressures.

Mechanisms that influence bacterial iron reduction at different HP conditions nevertheless remain unclear. Previous investigations on *Shewanella* genus have shown that multiheme *c*-type cytochromes (*c*-Cyts) in respiratory chain are involved in bacterial iron reduction (e.g., Shi *et al.*, 2007; Fredrickson *et al.*, 2008), and the respiratory components likely changed at high HP (Yamada *et al.*, 2000; Tamegai *et al.*, 2011). A pressure-regulated operon has been found in *S. benthica* and *S. violacea*, further supporting the influence of external HP on bacterial respiratory chain (Kato & Qureshi, 1999). Model simulations also showed that increasing pressures reduced the energy yield of all redox reactions examined except those involved in iron reduction (Fang *et al.*, 2010). Recently, we have investigated the behavior of enzymatic Fe(III) reduction-related *c*-Cyts at elevated HP by constructing *c*-Cyts mutants of strain WP3 (e.g., Δ*mtrA*, *B*, *C* and Δ*cymA)*, and the preliminary results indicated a pressure dependence of *c*-Cyts (data not shown). This suggests that the pressure effects on iron reduction could have responses from the enzymatic Fe(III) reduction proteins such as *c*-Cyts. Figure 2 shows that iron reduction by WP3 may occur at a maximum pressure of ~68 MPa, equivalent to water depth

Table 1 X-ray diffraction (XRD) data of the three main crystal faces (311), (220), and (440) for magnetite products after 120-h incubation at 0.1, 5, 20, and 50 MPa

	(311)			(220)			(440)		
Sample (MPa)	Intensity*	Area†	FWHM‡	Intensity	Area	FWHM	Intensity	Area	FWHM
0.1	48.8	3024.8	1.0370	16.3	1213.2	1.2240	25.0	2001.5	1.3090
5	93.4	5439.7	0.9813	24.2	1408.3	1.0370	46.9	3368.4	1.1696
20	107.9	6295.7	0.9711	31.5	1779.9	0.9246	53.0	3433.5	1.0745
50	112.3	6256.3	0.9193	29.6	1748.7	0.9010	50.8	3317.7	1.0523

*Peak intensity, in relative counts; †peak area; and ‡full width at half maximum of the peak.

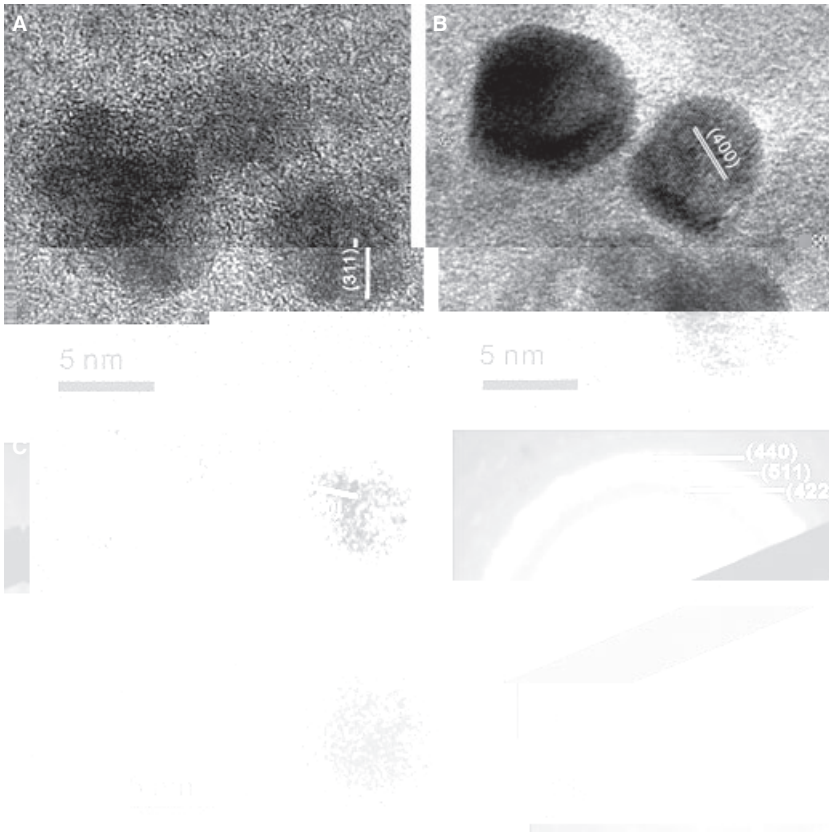

Fig. 8 High-resolution transmission electron microscopy images of the products at 5 MPa (A), 20 MPa (B), and 50 MPa (C), and selected area electron diffraction pattern of the 20 MPa products (D) after 120-h incubation.

of ~6800 m. This implies a possible pressure induced shut-off of enzymatic Fe(III) reduction under at this pressure. WP3 cells may then turn to other respiration pathways at high pressures to survive.

Effects of hydrostatic pressures on the biomineralization of magnetite

Our results show that nano-sized magnetite precipitation occurred when WP3 was cultivated at the four pressure conditions (0.1, 5, 20, and 50 MPa). Room- and low-temperature magnetic measurements on the 72-h biomineral products showed a decrease in M_s and M_{rs}, and an increase in B_c and B_{cr} with pressure (Figs 4 and 5). This trend consistently indicates less magnetite precipitation along with the increase in pressure due to the decreased cell growth rates and iron reduction rates and extent.

X-ray diffraction, HR-TEM, and rock magnetic analyses indicate that the crystallinity and grain size of magnetite particles formed at the experimental pressures appear to increase with pressure (Figs 5–8). Recently, Yazdani & Edrissi (2010) conducted coprecipitation chemical synthesis of magnetite at various pressures, and they observed an increase in grain size with pressure up to 0.6 MPa, which was attributed to the increase in Gibbs free energy change at higher pressures. XRD pattern of the magnetite products in the present study showed that the peak intensity increased, while the FWHM decreased at high-pressure

Table 2 Colony-forming units (CFU)-normalized iron reduction capability of WP3

Pressure (MPa)	Iron reduction (mM $CFU^{-1}h^{-1}$)
0.1	3.58×10^{-15}
5	4.84×10^{-15}
20	5.03×10^{-15}
50	3.11×10^{-14}

conditions (Fig. 7 and Table 1). At 0.1 MPa, the lattice constant was 8.4059 Å, larger than that of the theoretical value for stoichiometric magnetite (8.3967 Å). Magnetite formed by *S. algae* BrY after 265 h also had a lattice constant (8.4164 Å) larger than stoichiometric magnetite, which may be due to the incorporation of excess Fe(II) (Li *et al.*, 2009, 2011). Fast Fe(III) reduction and magnetite precipitation by WP3 at low HP may favor the accumulation of more Fe(II) in magnetite crystallization.

Iron carbonate minerals like siderite were expected in the reaction system, as precipitation of siderite consumes the CO_2 formed in reaction equation 1 and would decrease the volume. However, no siderite was detected in XRD pattern, HR-TEM images and rock magnetic measurements in our experiments. This may be explained by (i) CO_2 produced during iron reduction does not exceed the saturation needed for precipitation with Fe(II) as siderite in the culturing medium buffered with HEPES; or (ii) Fe(II) formed has a preference for magnetite precipitation in the pH-Eh condition (Wu *et al.*, 2011).

Implications for iron cycling in deep-sea environments

In deep-sea ecosystems, where oxygen is usually limited, bacterial iron reduction and precipitation of iron minerals may play significant roles in iron cycling and magnetic signals of sediments. Previous studies have shown that colloidal iron was widely distributed at water depth down to 5000–6000 m in North Atlantic and North Pacific (Wu *et al.*, 2001). High iron concentrations (300–400 μM) were detected in the pore waters of Puget Sound deep sediments (Stapleton *et al.*, 2005). Ferrihydrite minerals are widely detected in environments from freshwater to marine systems, as well as aquifers to hydrothermal water. The present study shows that *S. piezotolerans* WP3 is able to reduce ferrihydrite at pressures at least up to 50 MPa, corresponding to water depths of 5000 m. It suggests that WP3 could be extensively involved in iron biogeochemical cycling in deep-sea environments. The data of CFU-normalized iron reduction capability showed in this study provide us with constraints on bacterial contribution by marine IRB to the iron reduction and cycling in marine environments of different water depths.

Several recent studies of bacterially induced mineralization have suggested that IRB may contribute to the deposition of iron minerals in banded iron formations (BIFs). IRB could reduce Fe(III) and induce the precipitation of nanosized magnetite minerals at the presence of silicon (Percak-Dennett *et al.*, 2011). Under high-pressure conditions these biogenic nanoparticles can grow and form large magnetite crystals observed in BIFs during abiotic alteration (Li *et al.*, 2013). It was estimated that dissimilatory iron reduction as well as fermentation processes could account for the recycling back of 70% biologically formed Fe(III) (Konhauser *et al.*, 2005). Experiments of the present study showed that deep-sea *S. piezotolerans* WP3 could induce nanosized magnetite mineralization at HP of 50 MPa (the maximum pressure tested in this study). This finding further implicates the role of marine IRB in the deposition of iron minerals in BIFs via a demonstrated ability for this reaction to occur at deep-sea hydrostatic pressures. Moreover, as SP magnetite has high magnetic susceptibility, these nanosized magnetite minerals, if preserved, may contribute to magnetic signals of deep-sea sediments.

ACKNOWLEDGMENTS

We thank Xuegong Li and Zhongyuan You for valuable help in the HP experiments, Xiaoqing He for TEM analysis, and Elizabeth D. Swanner for polishing the language. We are grateful to three anonymous reviewers for their comments on the manuscript. This study was supported by the CAS/SAFEA international Partnership Program for the Creative Research Teams (KZCX2-YW-T10), National Basic Research Program of China (Grant No. 2011CB808800), NSFC Grants (40821091, 41240028 and 31290232) and CAS Graduate Science and Technology Creative Project.

REFERENCES

Dearing JA, Bird PM, Dann RL, Benjamin SF (1997) Secondary ferrimagnetic minerals in Welsh soils: a comparison of mineral magnetic detection methods and implications for mineral formation. *Geophysical Journal International* **130**, 727–736.

Fang J, Zhang L, Bazylinski DA (2010) Deep-sea piezosphere and piezophiles: geomicrobiology and biogeochemistry. *Trends in Microbiology* **18**, 413–422.

Fredrickson J, Romine M, Beliaev A, Auchtung J, Driscoll M, Gardner T, Nealson K, Osterman A, Pinchuk G, Reed J (2008) Towards environmental systems biology of Shewanella. *Nature Reviews Microbiology* **6**, 592–603.

Heimann A, Johnson C, Beard B, Valley J, Roden E, Spicuzza M, Beukes N (2010) Fe, C, and O isotope compositions of banded iron formation carbonates demonstrate a major role for dissimilatory iron reduction in ~2.5 Ga marine environments. *Earth and Planetary Science Letters* **294**, 8–18.

Johnson CM, Beard BL, Klein C, Beukes NJ, Roden EE (2008) Iron isotopes constrain biologic and abiologic processes in banded iron formation genesis. *Geochimica et Cosmochimica Acta* **72**, 151–169.

Kato C, Qureshi MH (1999) Pressure response in deep-sea piezophilic bacteria. *Journal of Molecular Microbiology and Biotechnology* **1**, 87–92.

Konhauser KO, Newman DK, Kappler A (2005) The potential significance of microbial Fe(III) reduction during deposition of Precambrian banded iron formations. *Geobiology* **3**, 167–177.

Li YL, Pfiffner SM, Dyar MD, Vali H, Konhauser K, Cole DR, Rondinone AJ, Phelps TJ (2009) Degeneration of biogenic superparamagnetic magnetite. *Geobiology* **7**, 25–34.

Li YL, Konhauser KO, Cole DR, Phelps TJ (2011) Mineral ecophysiological data provide growing evidence for microbial activity in banded-iron formations. *Geology* **39**, 707–710.

Li YL, Konhauser KO, Kappler A, Hao XL (2013) Experimental low-grade alteration of biogenic magnetite indicates microbial involvement in generation of banded iron formations. *Earth and Planetary Science Letters* **361**, 229–237.

Lovley DR (1997) Microbial Fe(III) reduction in subsurface environments. *FEMS Microbiology Reviews* **20**, 305–313.

Lovley DR, Holmes DE, Nevin KP (2004) Dissimilatory Fe(III) and Mn(IV) Reduction. *Advances in Microbial Physiology* **49**, 219–286.

Madsen DE, Hansen MF, Mørup S (2008) The correlation between superparamagnetic blocking temperatures and peak temperatures obtained from ac magnetization measurements. *Journal of Physics: Condensed Matter* **20**, 345209.

Moskowitz BM, Frankel RB, Bazylinski DA (1993) Rock magnetic criteria for the detection of biogenic magnetite. *Earth and Planetary Science Letters* **120**, 283–300.

Muxworthy AR, Williams W (2008) Critical superparamagnetic/single-domain grain sizes in interacting magnetite particles: implications for magnetosome crystals. *Journal of the Royal Society Interface* **6**, 1207–1212.

Nelson JB, Riley D (1945) An experimental investigation of extrapolation methods in the derivation of accurate unit-cell dimensions of crystals. *Proceedings of the Physical Society* **57**, 160–177.

Percak-Dennett EM, Beard BL, Xu H, Konishi H, Johnson CM, Roden EE (2011) Iron isotope fractionation during microbial dissimilatory iron oxide reduction in simulated Archaean seawater. *Geobiology* **9**, 205–220.

Picard A, Testemale D, Hazemann JL, Daniel I (2012) The influence of high hydrostatic pressure on bacterial dissimilatory iron reduction. *Geochimica et Cosmochimica Acta* **88**, 120–129.

Roh Y, Gao H, Vali H, Kennedy D, Yang Z, Gao W, Dohnalkova A, Stapleton R, Moon J, Phelps T (2006) Metal reduction and iron biomineralization by a psychrotolerant Fe(III)-reducing bacterium, *Shewanella sp.* strain PV-4. *Applied and Environmental Microbiology* **72**, 3236–3244.

Shi L, Squier T, Zachara J, Fredrickson J (2007) Micro Review: respiration of metal (hydr) oxides by *Shewanella* and *Geobacter*: a key role for multihaem *c*-type cytochromes. *Molecular Microbiology* **65**, 12–20.

Slobodkin A, Campbell B, Cary SC, Bonch-Osmolovskaya E, Jeanthon C (2001) Evidence for the presence of thermophilic Fe(III)-reducing microorganisms in deep-sea hydrothermal vents at 13° N (East Pacific Rise). *FEMS Microbiology Ecology* **36**, 235–243.

Stapleton RD Jr, Sabree ZL, Palumbo AV, Moyer CL, Devol AH, Roh Y, Zhou J (2005) Metal reduction at cold temperatures by *Shewanella* isolates from various marine environments. *Aquatic Microbial Ecology* **38**, 81–91.

Stookey L (1970) Ferrozine—a new spectrophotometric reagent for iron. *Analytical Chemistry* **42**, 779–781.

Tamegai H, Ota Y, Haga M, Fujimori H, Kato C, Nogi Y, Kawamoto J, Kurihara T, Sambongi Y (2011) Piezotolerance of the respiratory terminal oxidase activity of the piezophilic *Shewanella violacea* DSS12 as compared with non-piezophilic *Shewanella* species. *Bioscience, Biotechnology, and Biochemistry* **75**, 919–924.

Toffin L, Bidault A, Pignet P, Tindall BJ, Slobodkin A, Kato C, Prieur D (2004) *Shewanella profunda* sp nov., isolated from deep marine sediment of the Nankai Trough. *International Journal of Systematic and Evolutionary Microbiology* **54**, 1943–1949.

Wang F, Xiao X, Ou HY, Gai YB, Wang FP (2009) Role and regulation of fatty acid biosynthesis in the response of *Shewanella piezotolerans* WP3 to different temperatures and pressures. *Journal of Bacteriology* **191**, 2574–2584.

Wu J, Boyle E, Sunda W, Wen LS (2001) Soluble and colloidal iron in the oligotrophic north Atlantic and north Pacific. *Science* **293**, 847–849.

Wu WF, Li B, Hu J, Li JH, Wang FP, Pan YX (2011) Iron reduction and magnetite biomineralization mediated by a deep-sea iron reducing bacterium *Shewanella piezotolerans* WP3. *Journal of Geophysical Research* **116**, G04034.

Xiao X, Wang P, Zeng X, Bartlett D, Wang F (2007) *Shewanella psychrophila* sp. nov. and *Shewanella piezotolerans* sp. nov., isolated from west Pacific deep-sea sediment. *International Journal of Systematic and Evolutionary Microbiology* **57**, 60–65.

Xu Y, Nogi Y, Kato C, Liang Z, Rüger HJ, De Kegel D, Glansdorff N (2003) *Psychromonas profunda* sp. nov., a psychropiezophilic bacterium from deep Atlantic sediments. *International Journal of Systematic and Evolutionary Microbiology* **53**, 527–532.

Yamada M, Nakasone K, Tamegai H, Kato C, Usami R, Horikoshi K (2000) Pressure regulation of soluble cytochromes *c* in a deep-sea piezophilic bacterium, *Shewanella violacea*. *Journal of Bacteriology* **182**, 2945–2952.

Yazdani F, Edrissi M (2010) Effect of pressure on the size of magnetite nanoparticles in the coprecipitation synthesis. *Materials Science and Engineering* **171**, 86–89.